buildings

MDPI

Article

Nano-Zirconia as a Protective and Consolidant Material for Marble in Architectural Surfaces

Matea Urbanek [1,*], Teba Gil-Díaz [2,3,*], Johannes Lützenkirchen [3] and Valter Castelvetro [4]

[1] Materials Testing Institute, University of Stuttgart, 70569 Stuttgart, Germany
[2] Institute of Geosciences, Friedrich Schiller University Jena, 07749 Jena, Germany
[3] Institute for Nuclear Waste Disposal, Karlsruhe Institute of Technology, 76344 Eggenstein-Leopoldshafen, Germany; johannes.luetzenkirchen@kit.edu
[4] Department of Chemistry and Industrial Chemistry, University of Pisa, 56124 Pisa, Italy; valter.castelvetro@unipi.it
* Correspondence: matea.urbanek@mpa.uni-stuttgart.de (M.U.); teba.gil-diaz@kit.edu (T.G.-D.)

Abstract: Natural weathering of carbonate building surfaces exposed to outdoor conditions can be effectively tackled by appropriate products. The aim of this experimental study was to evaluate the effectiveness of nano-zirconia (n-ZrO_2) as a consolidant for calcite surfaces. Sorption kinetics were investigated in batch experiments by applying aqueous dispersions of n-ZrO_2 onto model, crushed Apuan marble samples of different bead sizes. Adsorption and desorption by the action of simulated rainwater as an environmentally relevant leaching solution were investigated. Adsorption studies revealed a good chemical affinity between n-ZrO_2 and calcite, while desorption resulted in <6% release of n-ZrO_2 and 100-fold lower solubility for 1 mm-sized beads compared to controls. These results suggest that n-ZrO_2 may adsorb efficiently to calcite and protect the surface from dissolution. The results of further tests performed on artificially aged and consolidated samples of Apuan marble indicate that the application of n-ZrO_2 only moderately affects water vapor permeability, water absorption coefficient, and drying behaviour. Therefore, no harmful effects are expected from the treatment. Micromechanical tests showed slightly increased mechanical strength after treatment. The obtained results highlight the effectiveness of n-ZrO_2 as a surface consolidant and protective agent for calcite.

Keywords: nanoparticles; sorption kinetics; inductively coupled plasma mass spectrometry; zeta-potential; built heritage; natural stone; treatment performance

Academic Editor: Emilia Vasanelli

Received: 12 December 2024
Revised: 24 January 2025
Accepted: 27 January 2025
Published: 5 February 2025

Citation: Urbanek, M.; Gil-Díaz, T.; Lützenkirchen, J.; Castelvetro, V. Nano-Zirconia as a Protective and Consolidant Material for Marble in Architectural Surfaces. *Buildings* **2025**, *15*, 492. https://doi.org/10.3390/buildings15030492

1. Introduction

White crystalline marble is one of the widespread materials used for sculptural work and built heritage. Environmental exposure is responsible for chemical and petrophysical changes occurring on this stone. The decay patterns observed on marble, particularly in highly polluted urban areas, can reach forms of degradation classified as sugaring or powdering [1], which implies severe loss of mechanical strength and accelerated surface erosion. For such reasons, it is not surprising that facades and sculptural work made out of marble need restoration and conservation care. To revert the loss of cohesion between grains, application of a stone consolidant may be necessary. Products in use for this purpose range from inorganic materials (e.g., hydroxyapatite, calcium hydroxides, ammonium oxalate, etc.) to synthetic polymers (e.g., acrylics) or hybrid systems such as organosilica or its precursors alkoxy- and alkylalkoxy-silanes [2]. Among them, the low molecular weight silane-based systems undergo polycondensation reactions to produce a silica or

organosilica gel and eventually a strongly adhesive layer; therefore, they are commonly used to consolidate stone [3]. However, because of the volume shrinking and embrittlement occurring upon sol-gel-type polycondensation, alkoxysilanes present some limitations, like cracking or poor chemical bonding to carbonate substrates. Such limitations contributed to the development of particle-modified and multifunctional consolidants [4–6]. Unfortunately, much of the current research is limited to the laboratory, and the developed products rarely reach the market which would make them more easily available for application onto the monument's surfaces or other artefacts where they are needed. The European Union (EU) has made efforts in the last decades to support industry-based research on conservation of the built heritage and promote the development of innovative materials. This is exemplified by past EU-funded projects such as Stonecore, Nanomatch, Nanorestart, or Nano-Cathedral. As some of the names imply, many of the newly engineered products are nanometric-based systems.

Nanotechnology is commonly applied in paints, coatings, and sealants for protecting different building surfaces from stain, scratch, or water adsorption, amongst others [7]. The most frequently engineered nanoparticles (ENPs) used as facade protective agents are silver/silver oxide (Ag/Ag_2O), titanium dioxide (TiO_2), zinc oxide (ZnO), and silicon dioxide (SiO_2) due to their capabilities in UV shielding, water and dirt repellence, and antimicrobial properties [8,9]. In addition, some ENPs are studied and used as effective consolidants, like calcium hydroxide ($Ca(OH)_2$), silicon dioxide, calcium carbonate ($CaCO_3$) polymorphs, and zirconia (ZrO_2) [10–12]. The advantage of consolidating with ENPs should lie in a more reactive surface and thus possibly better bonding to the substrate, their abilities to penetrate smaller pores, and even to prevent environmental degradation processes due to their functionality [13].

To assess the efficiency of a newly developed consolidant, different methods can be employed. The primary focus of consolidants is to restore the loss of cohesion and re-establish the physical properties of the weathered substrate. Therefore, mechanical tests are used to determine the effectiveness of treatments, often in combination with scanning electron microscopy (SEM) to analyse the microstructural features of the consolidated substrate. The issue of creating high-strength materials capable of resisting aggressive environments is engaged not only in architectural preservation but also in construction, geotechnical engineering, and other fields [14–16]. Furthermore, chemical compatibility with the substrate should be considered. Among the main properties of the treated stone that need to be pursued are a smooth mechanical depth profile, no drastic reduction of water vapour permeability, and mild visual changes. Only a few studies provide insight into the surface-consolidant chemical compatibility related to the interfacial bonding interaction. This information is relevant to better understand the effectiveness of the consolidants. For well-known systems like alkoxysilane and siliceous sandstone, there seems to be a wide acceptance that Si-O-Si bonds are formed between the substrate and the silica gel [17]. However, for many stone consolidating materials, knowledge and studies that deal with sorption or chemical bonding are still missing. In fact, while adsorption and interfacial interaction at the microscopic level impact macroscopic properties such as cohesivity and chemical compatibility, desorption can play a critical role when considering durability and environmental aspects of newly developed materials intended for such long-term applications.

Once in the built environment, ENPs may be released from the surfaces and transported via surface leaching/runoff (e.g., by rainwater) to surface waters, soil, and groundwater, where they may present their original properties or undergo chemical and/or physical transformations (i.e., according to the individual ENPs reactivity [18,19]). Both the direct release of ENPs and the potential dissolution of the contained metal ions are of

environmental concern in aquatic systems, especially in the case of biocidal ENPs and the potentially bioavailable Au, Zn, Ag, Cu, and Ti forms [20,21]. Studies concerning leaching of TiO_2 and Ag/Ag_2O from paints on outdoor surfaces [22–24] and modelling of ENPs mobility with rainwater runoff from building facades or within aquatic systems [25,26] have increased in the last years, prompted by growing concern about emerging environmental pollutants resulting in the release of new regulations [27,28]. Even though several studies have documented the presence of ENPs in industrial and municipal solid waste leachates, including landfills [29,30], ENPs are not systematically monitored in the environment [31]. Thus, there is still little knowledge about the release rates of ENPs under natural conditions [32] and their environmental risk assessment [28].

This environmental knowledge is even scarcer for zirconium-based nanoparticles [21], appropriate ENP candidates for consolidating stone materials in building facades given their general inert/biocompatible chemical properties and their high mechanical strength. Nano-ZrO_2 is mostly used in dentistry and ceramic powders, for which studies on their surface properties have generally shown higher absolute values of zeta-potentials (e.g., [33,34]) compared to those encountered in leachate suspensions from commonly used ENPs in paints (i.e., generally within $\pm$30 mV indicating flocculation [35]). Nevertheless, the effective toxicity of n-ZrO_2 remains unclear, given that ecotoxicological studies have shown both no effect (e.g., no impact on plant growth-promoting rhizobacteria in soils [36]) and significant effects for both nanoparticles and dissolved Zr-based complexes (e.g., impact on bacterial growth [37]). The potential benefits of n-ZrO_2 used as a stone consolidant in the built heritage are: (i) the nano-sized particles are typically characterized by a higher reactivity and finer surface roughness due to their higher specific surface area (surface/volume ratio), both providing improved adhesion to the substrate, along with better penetration in a porous material; (ii) due to the absence of crystallization or polymerisation processes (as it is the case for solutions of organic or inorganic low molecular weight species, or of organic/hybrid liquid precursors such as alkoxysilanes), low shrinkage and good bridging capacity are expected; (iii) the curing time is practically completed with the evaporation of water; (iv) water as a dispersion solvent is more environmentally friendly than alcohol, typically used for e.g., alkoxysilane-based consolidants.

The aim of this work was to analyse the reactivity of n-ZrO_2 on calcite (i.e., Apuan marble) in simulated natural conditions in order to understand the interaction between the newly engineered consolidants with crystalline marble for purposes of built-heritage preservation. This study was performed via adsorption and desorption batch experiments in two contrasting conditions (i.e., simulating onsite consolidant application with diluted solutions during adsorption and simulated rainwater for desorption) with two different particle sizes of marble (i.e., 0.25 mm and 1 mm) and two solid-liquid ratios (i.e., between the marble and the exposed solution, of 100 and 200 g/L). Three different consolidant dilutions (d100, d1000, and d10,000) were tested (i) to explore the chemical compatibility between the surface area and the amount of consolidants and (ii) to obtain insights on the leaching capability of the applied ZrO_2 nanoparticles into water systems (environmental risk assessment). As the n-ZrO_2 studied is a newly engineered product, additional aspects of the work involved the determination of treatment performance, including the analysis of mechanical strength gain, changes in water-based behaviour and, electrokinetical characterisations of the systems.

2. Materials and Methods

2.1. Characterisation and Preparation of the Substrate

Apuan marble is a white crystalline lithotype quarried from the Apuan Alps in Italy, often referred to as Carrara marble from the province where most of this metamorphic rock

is extracted [38]. It mainly consists of calcite (approx. 99 wt.%), with traces of quartz and dolomite (<1 wt.%), and it is known for its high strength (uniaxial compressive strength from 123 to 172 MPa) and durability related to its low Hg-porosity (approx. 0.6%). Thermal effects play an important role in Apuan marble degradation due to the highly anisotropic thermal expansion coefficient of calcite [39]. When severe degradation occurs, granular disintegration is commonly observed. As Apuan marble is a fine-grained lithotype, its surface-to-volume ratio increases significantly when inter- and intragranular cracks occur, often propagating into sheet-like intergranular spaces [3] that need to be restored in terms of their cohesion.

In the present study, two forms of Apuan marble were employed as test materials, that is, as granular aggregates for sorption studies and in monolithic form to assess treatment performance through various physical tests. For sorption studies, it was desired to increase the surface area of the material for better resolution in kinetic experiments, which is why the marble was crushed into chunks and then grinded for 30 s in a planetary ball mill (Fritsch Pulverisette 9 Vibrating Cup Mill). Afterwards it was wet sieved with the help of a mechanical shaker, using a set of sieves with 2.0 mm, 1.0 mm, 0.5 mm, and 0.25 mm mesh. Two sieve fractions were selected for the subsequent experiments: the fraction from 0.25 to 0.5 mm (hereafter labelled "0.25 mm sample") and the one from 1 to 2 mm (hereafter labelled "1 mm sample"). The obtained fractions were dried at 60 °C, allowed to equilibrate under laboratory conditions, and then stored in sealed high-density polyethylene containers.

Surface area measurements (Brunauer-Emmett-Teller, or BET, method) were performed using the model Sync 200 3p-Instruments Analyzer (from 3P Instruments GmbH and Co., KG, Odelzhausen, Germany) using N_2. The measured specific surface area of the two selected fractions was 0.440 $m^2\ g^{-1}$ and 0.149 $m^2\ g^{-1}$ for the 0.25 mm sample and the 1 mm sample, respectively.

In addition to the batch sorption experiments, visual, physical, and water-related tests were also performed on artificially aged and consolidated samples of Apuan marble in order to test treatment performance. The main reason for the artificial ageing of test specimens prior to consolidation is that Apuan marble in its pristine condition can be classified as a water-hindering material, which limits a laboratory-based study of treatment performance as no consolidant is able to penetrate the substrate. Therefore, a very common way to decrease the soundness of the material is by inducing microcracks into its fabric by heat stresses [40]. For this purpose, the specimens were placed in an electrically heated chamber furnace model Heraeus K 114 (3.5 L in volume, by Thermo Scientific, Waltham, MA, USA). The experimental setup for the heat treatment, as defined after an experimental pre-screening [41], involved three heat treatment cycles at a static peak temperature of 600 °C (heating from room to the peak temperature at 40 °C min^{-1}, followed by an isothermal step of one hour). Subsequent cooling to approx. 35 °C with an open front door of the chamber was carried out before the next heating cycle was adopted. These samples were used for micromechanical tests as described in Sections 2.6 and 3.5.

2.2. Experimental Solutions: Nano-ZrO_2 and Simulated Rainwater

The aqueous dispersion of n-ZrO_2 used in this study is a commercial product developed as a stone consolidant by Tecnan–Technologia Navarra de Nanoproductos, S.L. (Navarra, Spain). The specific formulation, under the tradename ZR110 (NC-29C), had been developed within the 'Nano-Cathedral' project, funded by the European program Horizon 2020 Call NMP21-AC 646178. As an industrially developed product, details of its preparation are protected by a non-disclosure agreement. According to the manufacturer's data sheet, ZR110 is an 11 ± 0.5 wt. % aqueous colloidal dispersion of ZrO_2 NPs about 120 nm in size. The dispersion has a density of 1.09 g/mL, a viscosity of 7 cP, and

a conductivity of 5.84 mS/cm. The strengthening effect is achieved upon drying of the treated substrate, when the nanoparticles within the porous stone build bridging structures between detached stone grains. For the adsorption experiments, the original ZrO_2 NP dispersion was diluted in deionized water (Milli-Q® water 18.2 MΩ cm^{-1}) as described in Section 2.3.

Simulated rainwater was prepared following the characteristic composition of average annual rainfall in northern Europe [42]. Briefly, a solution composed of a mixture of salts (Table 1) was prepared in Milli-Q® water, resulting in a working solution with an ionic strength of 0.082 mM and a pH of 5.9.

Table 1. Composition of the simulated rainwater solution used during desorption experiments. The composition is based on average concentrations of element mixtures found in rainfall from northern Europe [42].

Salt Type	Concentration	Brand
Potassium sulphate (K_2SO_4)	1 µM	Normapur, VWR Chemicals
Sodium sulphate (Na_2SO_4)	7 µM	Normapur, VWR Chemicals
Sodium nitrate ($NaNO_3$)	4 µM	99.5%, Merck
Anhydrous calcium chloride ($CaCl_2$)	14 µM	ACS Chemicals
Magnesium chloride anhydrous ($MgCl_2$)	4 µM	99%, Alfa Aesar

2.3. Experimental Design: Adsorption/Desorption Batch Kinetics

Sorption experiments were conducted at 100 and 200 g/L solid/liquid ratios by mixing 5 g and 10 g of marble in 50 mL final volumes, respectively. For the adsorption experiments, different dilutions (i.e., 100, 1000, and 10,000 times) from the original consolidant concentration of 11 ± 0.5 wt.% ZR110 were tested (see Figure 1). Experimental controls during adsorption included marble dispersions in 1 mM KCl (i.e., no consolidant, to account for calcite dissolution kinetics) and the diluted consolidant solutions (i.e., no marble, to account for potential nanoparticle precipitation during sampling).

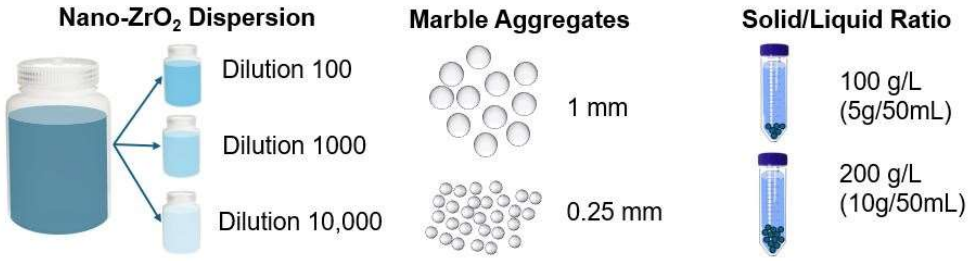

Figure 1. Schematic illustration of the batch experimental conditions accounted for during sorption experiments: Three different dilutions (d100, d1000, and d10,000) of the water-based n-ZrO_2 dispersion, two different bead sizes of crushed Apuan marble (1 mm and 0.25 mm), and two solid/liquid ratios (5 g or 10 g of crushed Apuan marble in 50 mL, corresponding to each of the specified n-ZrO_2 dilutions). In total, this resulted in 12 different initial conditions (3 dilutions × 2 bead sizes × 2 solid/liquid ratios) for the sorption experiments. After adsorption, the solutions were discarded, and the beads (with the different solid/liquid ratios and adsorbed n-ZrO_2) were reused for desorption studies, exposing the beads to 50 mL of simulated rainwater (see Table 1).

All dispersions were prepared in 50 mL BluCAPP polypropylene (PP) tubes. The dispersions were shaken over time in an overhead shaker (IKA® Trayster basic, Wilmington, NC, USA) and sampled at 0 min, 5 min, 15 min, 30 min, 1 h, 4 h, and 24 h after mixing the marble with the consolidant at different dilutions. Given the relatively high concentration of nanoparticles, solid-liquid separation was not possible either by filtering, due to filter

clogging resulting in high-pressure resistance, or by centrifugation, because of the risk of decanting nanoparticles, biasing the results. Therefore, the sampling strategy consisted of a systematic procedure of manual shaking (i.e., three shakes), then a settling/standing period of 5 s (i.e., enough time for the marble beads to visibly sediment to the bottom of the tube), followed by pipette collection of the upper 5 mL and acidification with 2% HNO_3 before analysis (15M Rotipuran® Ultra, Carl Roth, Karlsruhe, Germany). With this sampling procedure, the solid/liquid ratio was found to increase up to four-fold over time as the total volume is reduced while the marble bead mass remains nearly the same. This effect may result in enhanced adsorption behavior over time. Nevertheless, it is possible that these are representative conditions, potentially mimicking in-situ effects, e.g., evaporation of consolidant dispersion on building facades. At the end of the experiments, the supernatant was collected, and the remaining solids were covered (to avoid possible contamination) and oven-dried for 60 h at 60 °C (Memmert Trockenschrank ULM 600, 256 Liter, Carbolite Gero GmbH & Co., Neuhausen, Germany) to mimic on-site conditions (i.e., dry marble facades after treatment with commercial consolidant solutions) before subsequent batch desorption experiments.

Desorption experiments were carried out once by flooding with 50 mL of simulated rainwater (see Section 2.2) the oven-dried solids from the adsorption experiments. Controls of marble aggregates (marble without consolidant) and rainwater (rainwater without marble) were also included. Sampling at 0 min, 15 min, 30 min, 45 min, 4 h, and 24 h after mixing followed the same procedure adopted in the aforementioned adsorption experiments.

2.4. Quantification of ZrO_2 Nanoparticles

Samples collected from sorption experiments were digested with 50 µL of HF (42% ULTREX II, J.T. Baker) for two days. As there are no certified reference materials for ZrO_2 NPs, we used the experimental control samples as proxies for the digestion procedure. Both dissolved Ca and Zr concentrations were analysed after dilution in 2% HNO_3 (J.T. Baker ultrapure) via external calibration with a triple quadrupole inductively coupled plasma mass spectrometry (ICP-MS; iCAP-TQ, Thermo Scientific) in kinetic energy discrimination (KED)-mode (He). Potential interferences were checked for ^{91}Zr and ^{44}Ca (e.g., polyatomic influences of V and Si), but no corrections were required as the experimental concentrations were in the ppm range. Detection limits (LOD) for dissolved Zr and Ca concentrations were $6.8.10^{-3} \pm 4.3.10^{-3}$ µg/L and 5.6 ± 1.5 µg/L, respectively, for several analyses of 3 blanks involving 2% HNO_3 (J.T. Baker ultrapure, VWR, Radnor, PA, USA). Recoveries of analytical performance were 109 ± 1% for Ca (SPS-SW2) with an RSD (relative standard deviation) of 11% for the non-certified Zr. Digestion blanks (n = 2), used to control potential contaminations from the digestion processes, were max. 0.59 µg/L on Zr and 49 µg/L on Ca, i.e., at least 1 and 3 orders of magnitude below sample concentrations, respectively. The composition of the simulated rainwater also had little influence on the batch samples (i.e., $18.10^{-3} \pm 8.10^{-3}$ µg/L for Zr and 480 ± 13 µg/L for Ca).

2.5. Surface Characterisation: Nanoparticle Size, and Zeta-Potential

The size and size distribution of ZrO_2 nanoparticles were measured by dynamic light scattering (DLS) using a Brookhaven ZetaPlus Zeta Potential Analyzer (Brookhaven Instruments Corporation®, Nashua, NH, USA). Zeta (ζ) potentials were determined in two ways: (1) via DLS for the n-ZrO_2 properties and (2) via streaming current for Apuan marble surfaces.

Single-point ζ-potentials were determined via electrophoretic mobility (μ_E), Equation (1) with a NanoBrook 90Plus PALS (Brookhaven®) instrument by using Hückel's approximation (Equation (2)):

$$\mu_E = \frac{V_0}{E_0}; \quad (1)$$

$$\zeta = \frac{3}{2} \cdot \frac{\mu_E \eta}{\varepsilon}; \quad (2)$$

where V_0 is the terminal velocity, E_0 is the electrical field applied, μ_E is the measured electrophoretic mobility in $(\mu m/s)/(V/cm)$, η is the viscosity of the medium [Pa s], and ε [$F \cdot m^{-1}$] is the permittivity of the solution. These single points of ζ-potential measurements were used to characterise the electrostatic properties of the colloidal solution and account for its stability when diluted for purposes of sorption analysis.

Measurements of ζ-potential on flat macroscopic Apuan marble surfaces were performed on monolithic fresh test specimens with the SurPASS™ Electrokinetic Analizer (Anton Paar GmbH, Graz, Austria). The streaming current measurements were performed using the adjustable gap cell configuration. In this cell, the two flat walls of the slit through which the probing electrolyte solution flows consist of the surfaces of Apuan marble under investigation. The streaming channel amounts to 20 mm in length, 10 mm in width, and with a gap height that can be adjusted to assure proper flow conditions. The experimental conditions were as follows: (i) a 0.082 mM simulated rainwater as probing electrolyte, (ii) the simulated rainwater with titrated addition of up to 10 mM $CaCl_2$ to introduce potential determining ions (PDI) of calcite, and (iii) subsequent pH titration with HCl to evaluate for pH and salinity dependence. As a comparison, the ζ-potential of the Apuan marble was also determined in a 1 mM aqueous KCl solution. The pH titration was carried out in the range from 7.5 to 4.5 with a 0.05 M HCl solution using the automatic titrator module of the apparatus. All probing electrolytes were purchased from Sigma-Aldrich Chemie GmbH and were diluted to the target concentrations from a stock solution. The probing electrolyte solution was not purged with N_2 (a common procedure in conventional measurements aimed at removing any dissolved CO_2) to better simulate the batch experimental conditions.

The ζ-potential obtained from solid surfaces of Apuan marble, was calculated from streaming current data according to Equation (3):

$$\zeta(I_{Str}) = \frac{dI_{Str}}{d\Delta p} \frac{\eta}{\varepsilon_0 \varepsilon_r} \frac{L}{A}; \quad (3)$$

where η [Pa s] is the dynamic viscosity of the electrolyte, ε and ε_o are the dielectric constant of the electrolyte solution and the vacuum permittivity [8.854×10^{-12} $F \cdot m^{-1}$], respectively, ζ-(I_{str}) represents the ζ-potential derived from streaming current measurements and $\frac{dI_{Str}}{d\Delta_p}$ the streaming current coupling coefficient. The latter is experimentally obtained from the slope of the linear fit of streaming current [A] to pressure difference ramp [Pa].

2.6. Treatment Application and Treatment Performance

The consolidant in its original concentration was applied twice, with a pause of 24 h between each application, by means of rising capillary absorption for one hour. After treatment application, the specimens were placed in a loosely opened container to avoid quick drying and possible back migration of the ENPs. Table 2 displays the testing methods used to assess the efficiency of the treatment and its compatibility. All samples have been tested in their pristine, artificially aged, and subsequently consolidated conditions approx. one month after application.

Table 2. Laboratory-based test methods used to assess the success criterion of treatment performance and material properties.

Type of Test	Reference	Criterion and Characterisation
Scanning electron microscopy	Not std.	Bonding to substrate, bridging.
Pore size distribution	Not std.	No secondary micro porosity
Dynamic elastic modulus	EN 14146 [43]	Improvement
Drilling resistance	Not std.	Improvement, smooth profile
Water vapour permeability	EN 15803 [44]	No drastic reduction
Water absorption coefficient	EN 15801 [45]	No drastic reduction
Drying index	EN 16322 [46]	No drastic reduction
Contact angle of water	EN 15802 [47]	Change $\leq$ 20% untreated
Colour measurements	EN 15886 [48]	ΔE change < 5

As concerns the reproducibility and error analysis, the authors have used the size and number of specimens as well as data analysis in accordance with the respective European norms, referenced in Table 2. In the case of scanning electron microscopy, pore size distribution, and drilling resistance measurements, which are not standardised destructive or invasive techniques, the results should be viewed as indicative, providing hints that may or may not confirm other experimental evidence. Particularly for SEM image analysis, reproducibility and error analysis are highly challenging.

2.6.1. Scanning Electron Microscopy

A Quanta Feg 450 (FEI) scanning electron microscope was used to analyse polished cross sections and broken fragments of the consolidated stone specimens. In the cross sections, the bonding, spatial distribution, and bridging capacity of the cured consolidants were analysed. The analysed depth of the polished cross sections was up to 0.5 cm because the studied consolidant is intended to strengthen the surface and subsurface layers. The samples were embedded with the resin-hardener system XW 396/XW 397 with a mixing ratio of 10:3 (Huntsman Corporation, Salt Lake City, UT, USA). It was cured overnight at 40 °C. On the fragments, the top layer of the consolidant was investigated in terms of microstructure and topology. All samples were mounted on aluminium sample holders, coated with a 5 nm thick gold film prior to analysis, and observed at 20 kV accelerating voltage in backscatter and secondary electron mode. The cured consolidant is determined by its shape and grey values, which are distinct from the substrate. The latter is particularly visible in backscatter mode, since the chemical composition of the consolidant differs from that on the substrate, yielding a distinctive grey value. Observations concerning bonding sites, spatial distribution, and bridging of the cured consolidant should be viewed as indicative evidence and clues since only one sample was analysed, and SEM imaging is rather a descriptive and qualitative technique.

2.6.2. Mercury Intrusion Porosimetry

The porosimetric features of the substrate in all its conditions were determined by a porosimeter, Porotec Pascal 140/440 (Thermo Fisher Scientific Inc., Waltham, MA, USA). All measures were performed in duplicate to account for the uniformity of the same sample state. The size of the analysed sample amounted to $1 \times 1 \times 1$ cm^3.

2.6.3. Dynamic Elastic Modulus (Ultrasound)

The analysis of the longitudinal dynamic modulus of elasticity by means of the longitudinal resonance frequency was determined on prismatic specimens with dimensions of $1 \times 1 \times 4$ cm^3. As Young's modulus is determined on the same specimens before and after treatment, an average of three specimens is sufficient to assess whether any improve-

ment after consolidation is achieved. The device developed by Geotron-Elektronik (Pirna, Germany) consisted of an ultrasonic pulse generator (CONOSONIC C2-GS), a pair of transducers (UP-DW), and a notebook running the Light House Touch software. The Young's modulus [GPa] is obtained by Equation (4):

$$Ed_L = 4{\cdot}10^{-6}{\cdot}l^2{\cdot}{F_L}^2{\cdot}\rho; \quad (4)$$

where the calculated dynamic modulus of elasticity Ed_L is obtained through the longitudinal fundamental resonance frequency F_L, the specimen's length l, and the apparent density of the lithotype ρ.

2.6.4. Drilling Resistance Measurements

The resistance to a penetration force (reported in Newton) was assessed with the DRMS Cordless device from Sint Technology (Calenzano, Florence, Italy). A 3 mm diameter polycrystalline diamond bit drill was used to penetrate the sample up to 15 mm and analyse the state before and after treatment application. The speed of rotation was set at 600 rpm and the penetration speed at 10 mm/min.

2.6.5. Water-Related Tests (Water Vapour Permeability, Water Absorption Coefficient, Drying Behaviour, and Contact Angle)

According to the standard EN 15803, the water vapour permeability was assessed with the wet-cup system (cup type 1), filled with water. Three specimens were tested before and after the treatment. The cups, mounted with the specimens, were filled with water and placed in a climatic chamber (Heraeus Vötsch mod. VC3 4034, by Vötsch Industrietechnik GmbH, Balingen, Germany) set at 23 °C and 50% RH to equilibrate. Every 24 h the weight was recorded for at least one week. The results were plotted as the mass change versus time to obtain the slope of the linear section of the curve G [$kg{\cdot}s^{-1}$]. The water vapour permeance W_p [$kg{\cdot}m^{-2}{\cdot}s^{-1}{\cdot}Pa^{-1}$] was calculated according to Equation (5):

$$W_p = G{\cdot}A^{-1}{\cdot}{\Delta p_v}^{-1}; \quad (5)$$

where A is the test surface area in m^2 and Δp_v [Pa] stands for the water vapour pressure difference across the specimen. Subsequently, W_p was used to obtain the water vapour permeability δ_p [$kg{\cdot}m^{-1}{\cdot}s^{-1}{\cdot}Pa^{-1}$], according to Equation (6):

$$\delta_p = W_p{\cdot}D; \quad (6)$$

where D [m] is the mean specimen thickness.

The determination of the water absorption coefficient after one hour is reported in $kg{\cdot}m^{-2}{\cdot}h^{-0.5}$ and defined, therefore, as the amount of water in kg absorbed per square meter as a function of the square root of one hour. The test was carried out on three specimens with a dimension of $3 \times 3 \times 3\ cm^3$.

The determination of the drying behaviour allowed calculating the water loss of a saturated sample over time, i.e., one week for the present case. Prior to the test, samples were placed in a desiccator with silica gel to maintain constant humidity conditions at 23 ± 1 °C. The lateral sides of the samples were not sealed. Thus, the drying occurred from the entire surface. Three specimens with dimensions of $3 \times 3 \times 3\ cm^3$ were used to obtain the drying rate determined according to Equation (7):

$$M_i = \frac{m_i - m_f}{A} \quad (7)$$

The residual amount of water present in the specimen ($m_i - m_f$) per unit area (A, calculated from the entire surface) is expressed in kg·m^{-2} for a given time (t_i, in hours). According to this curve, the first and second drying phases can be plotted. Finally, the drying index IA is calculated from Equation (8):

$$IA = \frac{\int_{t_0}^{t_f} M_i dt}{M_{max} t_f}; \quad (8)$$

where M_i corresponds to water loss at t_i, M_{max} is the water at t_0, and t_f is the time taken as the end of the test (24 h). To evaluate the integral of the area below the curves, the software OriginPro2019 was used.

The water contact angle was determined with the Mobile Surface Analyzer from Krüss (Hamburg, Germany). An average of three sampling points was obtained on the surface of the marble specimens for the respective conditions.

2.6.6. Visual Inspection

The colour measurements have been performed on Apuan marble before and after treatment with a ColorLite sph 850 spectrophotometer (ColorLite GmbH, Katlenburg-Lindau, Germany). A D65 illuminant at 10° standard observer with a reflectance spectrum in the range of 400 to 700 nm was used. Three tests obtained at the same spot are reported as average values according to the International Commission on Illumination CIE L*, a*, b* colour parameters. The total colour difference (ΔE*) between artificially aged (a) and treated (t) samples is obtained from Equation (9):

$$\Delta E_{t,a}{}^* = \left[({L_t}^* - {L_a}^*)^2 + ({a_t}^* - {a_a}^*)^2 + ({b_t}^* - {b_a}^*)^2 \right]^{1/2} \quad (9)$$

where ΔL^* is the lightness difference, Δa^* the red/green difference, and Δb^* the yellow/blue difference.

3. Results and Discussion

3.1. Nano-ZrO_2 Dispersion Properties

The characterisation of the colloidal phase is important as it may support interpretations of sorption kinetics. Nanoparticle characterisation confirmed that the properties of the commercial consolidant product persisted in the diluted formulations used in this study. Nanoparticle sizes, characterised by DLS, ranged between 70 nm and 130 nm (with a polydispersity from 0.1 to 0.2) for the original and diluted dispersions, respectively. The pH of the original consolidant was 9.8, and that of the diluted solutions decreased with increasing dilution from 9.4 (d100) to 6.7 (d1000) and to values equivalent to pure water, that is, ~5 (d10,000, from atmospheric CO_2). Despite this dramatic decrease in pH for d10,000 samples, all pH values during the adsorption experiments were buffered at pH ~8 via calcite dissolution from the marble beads. This means that only the control samples of consolidant for d10,000 (i.e., only consolidant, no marble beads) may show different stability compared to the less diluted controls. In fact, the measured ζ-potentials of diluted consolidant solutions showed averages of -70.5 ± 2.6 mV (d100), -89.6 ± 2.5 mV (d1000), and -33.6 ± 1.5 mV (d10,000). Note that the ζ-potential of the original consolidant concentration was not quantified because the solution was not transparent enough for the measurement.

3.2. Electrokinetic Potential and Solubility of Apuan Marble in Selected Conditions

The value of ζ-potential for stones in different conditions and exposed to different electrolytes depends on both the stone and the testing solution. The multifactorial depen-

dence of the ζ-potential (e.g., instrument type, stone porosity, use of aggregates vs. solid samples, surface conductivity, presence of soluble salts, etc., to name a few) can make the interpretation of the results quite complex. Moreover, the behaviour of a stone in equilibrium with an electrolyte solution will differ from the one under non-equilibrium conditions. Likewise, stone resistance towards different acidic and basic conditions, the buffering capacity of carbonate, as well as the presence of potential determining ions (PDIs), will yield different results. The ζ values obtained within the present study are better interpreted as relative changes (trends) and not via absolute values, especially since the entire analysed system is in non-equilibrium. While a direct comparison of ζ obtained by means of electrophoretic mobility (for the colloidal suspension) and streaming current (for solid surfaces) measurements cannot be made, trends can indicate possible processes and explanations.

The testing conditions adopted in this study were defined based on their expected relevance for on-site situations to which the construction material is located and exposed to environmental conditions. As stone surfaces are cyclically exposed to rainwater, ζ alterations of the Apuan marble surface in simulated rainwater were studied (Figure 2a). The results reveal a time-dependent ζ change, starting from −10 mV at the beginning of the experiment and increasing in magnitude to −20 mV after ~14 h of exposure. After approx. 6 h of exposure, only minor further change of ζ and of the corresponding pH cooccurred, indicating a more stable condition. It should be noted that in order to reach equilibrium, the testing conditions (e.g., exposed surface area, amount of testing solution, open CO_2 system) need to be considered.

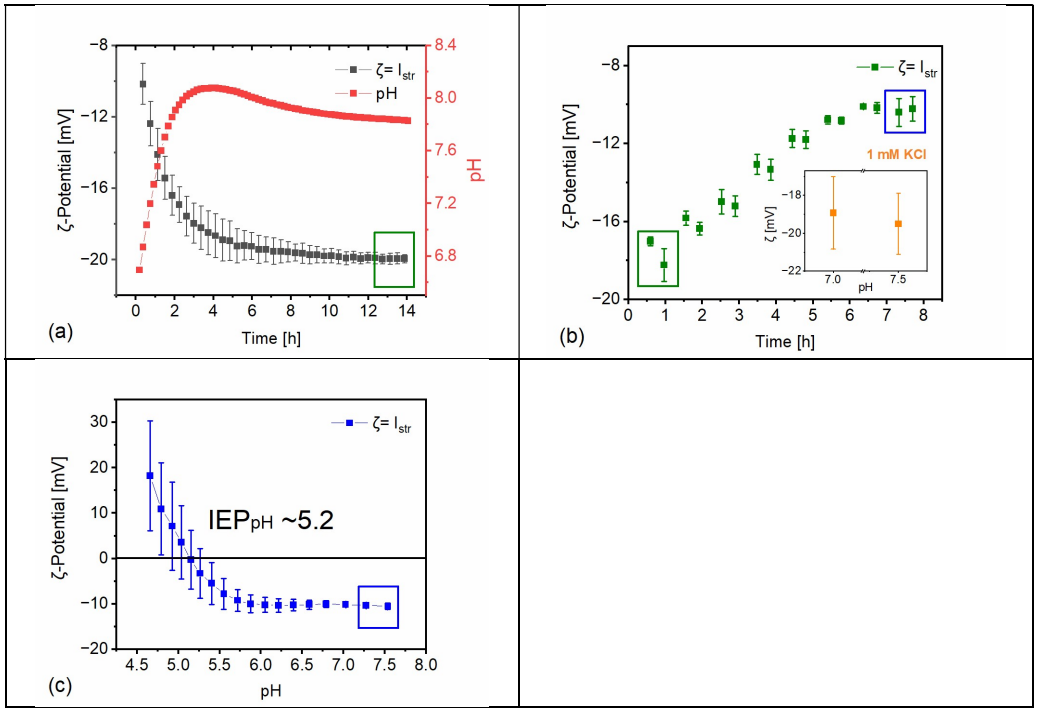

Figure 2. Electrokinetic potential alterations of Apuan marble in different conditions relevant for the present study. (**a**) Long-term ζ evolution for Apuan marble in simulated rainwater, with the corresponding change of pH. (**b**) Same conditions as before, but with a stepwise addition of $CaCl_2$ until 10 mM is reached. For comparison, the inset shows the ζ of an Apuan marble in a 1 mM KCl solution. (**c**) HCl titration from pH 7.5 to 4.5 in 10 mM $CaCl_2$-doped simulated rainwater solution until the pH and salinity-dependent isoelectric point was reached (ζ ≈ zero). Note that the green and blue marked rectangles display the end of one testing condition and the beginning of the subsequent testing conditions.

When the Ca^{2+} ions are added to the rainwater solution, Ca^{2+} ions are PDIs for the calcite surface; ζ decreases in absolute value (i.e., it becomes less negative) and shifts towards −10 mV after the addition of 10 mM $CaCl_2$ to the background solution. By comparing the first single-point measurements of ζ in simulated rainwater (−10 mV) with ζ in a 1 mM KCl solution (−20 mV), it is evident to what extent different aqueous solutions may affect the measured value of ζ (compare Figure 2a with the inset of Figure 2b). The addition of PDIs is insofar relevant as a naturally aged substrate might have more surface area exposed to rainwater due to partially lost cohesion of the substrate, corresponding to a partial loss of adhesive contact between grains (e.g., formation of microcracks), which directly influences the surface reactivity and the release of these ions from the mineral surface. Moreover, building construction sites are known to be contaminated by different salts in different concentrations, which makes the use of different electrolytes in varying concentrations relevant to real case exposure under environmental conditions.

After the addition of 10 mM $CaCl_2$ to the rainwater background electrolyte, a titration with HCl was conducted to obtain the pH and salinity-dependent isoelectric point (IEP_{pH}); see Figure 2c. The IEP_{pH} is the pH at which the ζ-potential is zero, that is, where an equal amount of positive and negative charges is present in the vicinity of the surface. The magnitude of ζ indicates the degree of electrostatic repulsion for similarly charged surfaces. The closer the measured system is to the IEP_{pH}, the more likely it is that two adjacent surfaces will attract each other. The titration of the system is relevant because the pH of water-based ENPs used in building heritage may span from highly alkaline (e.g., calcium hydroxide) to acidic (as in several sol-gel-based inorganic colloidal materials).

3.3. Sorption Kinetics of Nano-ZrO_2 onto Calcite Control Conditions

Consolidant controls during adsorption experiments over time showed reproducibility among the tested Zr concentrations and dilution factors. This means that (i) for a given dilution factor, dissolved concentrations of Zr were constant over time (i.e., there was no loss of n-ZrO_2 due to precipitation), and (ii) Zr concentration increased proportionally between dilution factors (e.g., Zr at d1000 is 10 times smaller than that of d100), as expected. The remaining diluted consolidant in the control samples was emptied, and the samples were reused during desorption studies to monitor n-ZrO_2 sorption onto the tube walls and potential redissolution onto the rainwater in 24 h. For the three tested dilutions, results show dissolved Zr concentrations of two to three orders of magnitude below the Zr concentrations obtained from desorption samples with calcite.

Corresponding controls of calcite beads in 1 mM KCl during adsorption experiments and in simulated rainwater during desorption experiments showed an overall dissolution in 24 h sorption experiments between 42 and 137%. However, there was no clear/specific dissolution pattern/trend related to the tested batch conditions: solid/liquid ratio (100 vs. 200 g/L) and bead size (1 mm vs. 0.25 mm). Noteworthy, based on the initial ionic strength of the calcite control samples at 1 mM KCl and those resulting from the dilution of the original consolidant dispersion (see Section 2.3), these controls are representative only of the calcite beads present in condition n-ZrO_2 d100. This is the experimental condition closest to in situ/real applications, where (given our results) calcite dissolution in the absence of a consolidant is expected. This also implies that experimental conditions with n-ZrO_2 d1000 and d10,000 could/should potentially show higher dissolution of calcite compared to the control. For this reason, in the following discussion, results of dissolved Ca pertaining to each experimental condition are reported in relative percentages, that is, comparing the concentrations obtained at time 0 and that at the end of the experiment (24 h) for each experimental condition, and not relative to the concentrations obtained in the control samples.

3.4. Sorption Affinity of Nano-ZrO_2 and Effect on the Dissolution of Calcite

Overall, sorption studies showed consistent adsorption of n-ZrO_2 and little desorption in rainwater conditions. Illustrative results for the case of d10,000 are shown in Figure 3. Given the wide range of experimental conditions tried in this work, we can report with confidence that adsorption studies revealed a good chemical affinity between n-ZrO_2 and calcite, adsorbing 50–75% of the added n-ZrO_2 in d10,000 (Figure 3a), 80–90% in d1000, and 14–90% in d100. Specifically, we obtained 14% sorption for the 1 mm beads at a 100 g/L solid/liquid ratio and 90% for the 0.25 mm beads and 200 g/L solid/liquid ratio. This was expected because smaller bead sizes imply larger surface areas and higher concentrations of beads provide more surface for the n-ZrO_2 to adsorb. However, for the other cases, the trend was consistent for the bead sizes but not for the solid/liquid ratio. As an example, for d10,000, we obtain around 50% adsorption with 1 mm beads and around 75% adsorption with 0.25 mm beads for both solid/liquid ratios. This can be related to incomplete digestions of n-ZrO_2 (unknown due to lack of certified reference materials) or experimental variability during sampling.

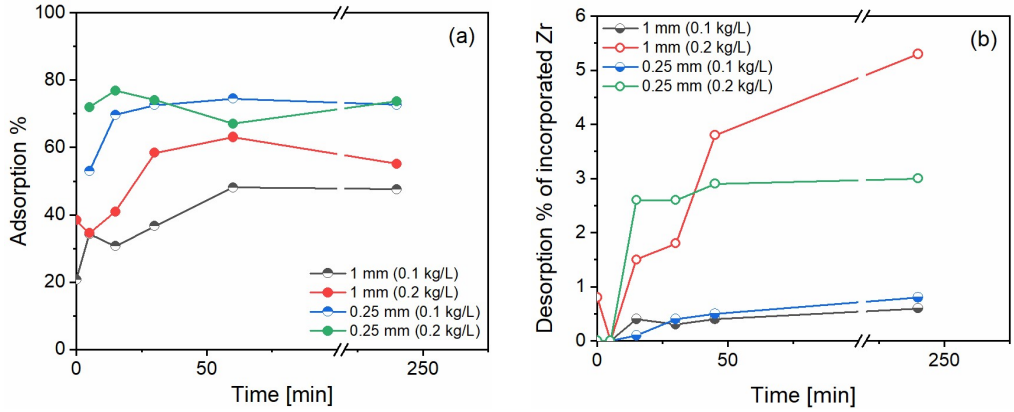

Figure 3. Adsorption for d10,000 (**a**) and desorption in simulated rainwater (**b**) for n-ZrO_2 on Apuan marble at two different bead sizes (i.e., 1 mm and 0.25 mm) and two different solid/liquid ratios (0.1 kg/L and 0.2 kg/L, corresponding to 100 g/L and 200 g/L, respectively).

Overall desorption of n-ZrO_2 in rainwater conditions was a maximum of 6% for calcite exposed to d10,000 (Figure 3b), 12% for calcite exposed to d1000, and 5% for calcite exposed to d100 n-ZrO_2. In all cases, the release of n-ZrO_2 doubled proportionally for the bead's concentration. As an example, for d1000, the conditions with 5 g of marble aggregates released 6% whereas the one with 10 g released 12%. The percentage desorbed corresponds to the concentration of Zr in the solution during desorption, divided by the amount of Zr lost from the solution to the surface during adsorption.

Regarding calcite solubility, for comparative purposes, Figure 4 shows the concentrations of dissolved Ca grouped for the cases of 0.25 mm beads (Figure 4a) and 1 mm beads (Figure 4b) over time for both adsorption (from minute 0 until minute 240) and desorption experiments (after minute 240). As a reference guideline, the corresponding dissolved Ca concentration of the controls of calcite (only truly comparable to d100 conditions) is also represented in both graphs. For better comparability, the timeline of adsorption/desorption experiments is represented one after the other, meaning that the plotted times respect the timeframes of the experiments but not a real temporal succession (i.e., desorption experiments did not start at 260 min after the beginning of adsorption experiments). These results suggest that, as expected, calcium dissolution from 0.25 mm beads was always higher than from 1 mm beads, for both controls and experimental conditions. The solid/liquid ratio also consistently influences the outcome, with higher dissolution of calcite for 200 g/L com-

pared to 100 g/L. These results suggest that, despite the seemingly high uptake of n-ZrO_2 onto calcite (e.g., Figure 3), the resulting effective calcite solubility is contrasting. During adsorption conditions, calcite solubility was generally reduced compared to the controls, with a consistent trend regarding n-ZrO_2 dilutions. However, the reduced solubility of calcite during desorption experiments seems to be an effect of the oven-drying performed between sorption experiments, as the control samples also showed less dissolved Ca compared to adsorption experiments. Nevertheless, there is an effective reduction in calcite dissolution with decreased dilution factor, especially for 0.25 mm bead sizes. This means that applied n-ZrO_2 in high concentrations not only remains within the calcite surface during exposure to simulated rainwater but also reduces significantly (e.g., up to 100-fold lower solubility) calcite dissolution. This effectiveness is higher with smaller calcite grain sizes. These results suggest that n-ZrO_2 may adsorb efficiently to calcite and protect the surface from dissolution.

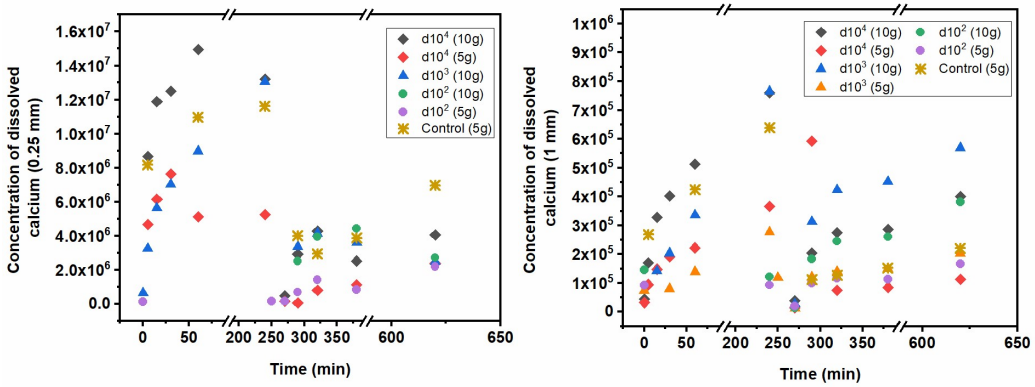

Figure 4. Concentrations of dissolved calcium in µg/L (comparing the concentrations obtained at minute 0 and after 24 h) for each experimental condition. Results are displayed for 0.25 mm beads (**a**) and 1 mm beads (**b**) over time for both adsorption (from minute 0 to minute 240) and desorption experiments (i.e., after minute 240). The specified marble mass corresponds to the solid-liquid ratio of 100 g/L (5 g in 50 mL) and 200 g/L (10 g in 50 mL).

The sorption and desorption experiments were exploratory, aiming at the investigation of a broad spectrum of experimental conditions rather than a large number of replicate experiments for statistical validation. Further replicate experiments are planned to provide more robust and targeted results and to validate the proposed innovative experimental approach. In any case, quality control via blank tests and triplicate ICP-MS analyses (RSD < 20% variability) confirmed the overall reliability of our results.

3.5. Efficiency and Compatibility of Nano-ZrO_2 for Purposes of Surface Consolidation

3.5.1. Scanning Electron Microscopy

SEM studies on polished cross sections indicate good bonding between calcite and zirconia (see Figure 5a). In fact, cohesive cracks were much more frequently observed within the consolidant layer than as adhesive detachment at the substrate-zirconia interface. Besides, the generated microcracks were filled with n-ZrO_2 without pore-clogging effects (i.e., complete filling of the cracks) as shown in Figure 5b. The surface micrographs taken from broken chips show the presence of some efflorescence over the texture of the cured consolidant (see Figure 5c); however, that feature may be related to microcrystals of a stabilising agent that was added to the colloidal dispersion during the manufacturing processes (see EDX analysis in Figure S1). Recent studies have reported on sols in alcohol and water dispersions to contain sodium chloride as a by-product of the preparation [49]. In general, such by-products might compromise the durability of the treatment and the

substrate. The topography of the cured and hardened zirconia displays a crackled surface, whereby it follows the roughness of the substrate (see Figure 5d). Drying stresses are known to cause cracking of inorganic consolidants [50]. The crackled consolidant on top of the marble surface displays a higher roughness and a higher surface area than the pristine marble surface, which probably contributes to NP release and enhanced leaching. Such undesirable effects might also have positive aspects, as in the case of photocatalytic TiO_2 nanoparticles with self-cleaning and depolluting properties [49]. The authors describe that a higher surface roughness and porosity make n-TiO_2 more easily available; therefore, the target pollutant NOx was degraded to a greater extent.

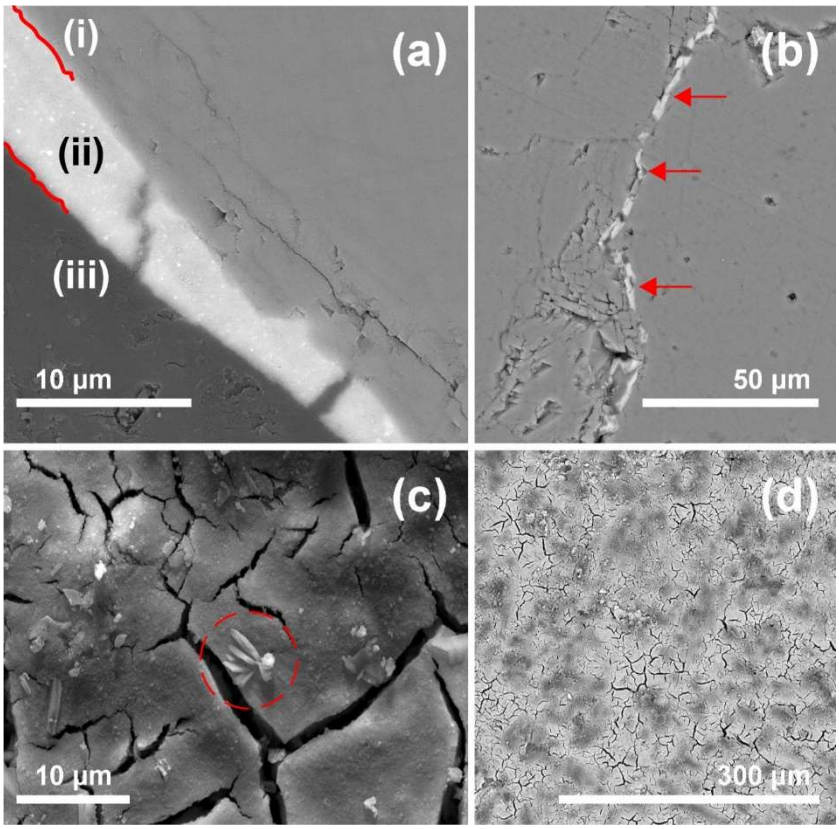

Figure 5. SEM micrographs displaying (**a**) the bonding between calcite (i) and zirconia (ii), while (iii) is the resin used for embedding the sample, (**b**) partial filling of microcracks, (**c**) topography of cured n-ZrO_2 with efflorescence (red circle), and (**d**) overview of the crackled consolidant on top of Apuan marble.

The bridging capacities of the n-ZrO_2 product cannot be evaluated properly as the cracks generated by heat treatment are very small and exhibit sheet-like intergranular openings. Equally challenging is the evaluation of the depth distribution of the NPs due to the typically very small pore size of this marble substrate, which prevents effective penetration of the aqueous n-ZrO_2 and results in rapid formation of a cured NP surface layer including only a thin sub-surface region. Thus, this product, depending on the pore structure of the substrate, should be considered as a surface strengthener (e.g., for the fine sheet-like openings of marble) rather than a bulk consolidant, as the latter should be capable of penetrating deeply and of increasing the bulk mechanical strength of the stone material. As only one sample per condition was analysed, the results should be viewed as initial pointers regarding the bonding and crack filling and, in general, on how the cured consolidant is distributed in the substrate.

3.5.2. Mercury Intrusion Porosimetry

The measurement of pore size distribution (PSD) by mercury intrusion porosimetry allows us to assess the changes in the pore network caused by ageing or by a treatment. The graphs in Figure 6a,b highlight the significant difference in the PSD, with a marked shift of the smaller sub-micrometre pores towards 1+ micrometre-sized pores, along with an increase in total Hg-porosity (from 0.7% to 3.6%) upon artificial ageing of the Apuan marble [51]. The treatment with n-ZrO_2 causes only moderate changes, as the comparison of Figure 6c clearly shows. The treatment appears to mostly affect the pores in the range below 0.1 µm, where deposition of the consolidant is more effective in occluding the pore and thus decreasing the total open porosity from 3.6% to 2.9%. To obtain statistically relevant pore size distribution data, more samples in each condition should be analysed. The results indicate that there is no severe change in the pore structure as a result of the application of n-ZrO_2, which can be viewed as a surface-strengthening and protecting agent even if chemically heterogeneous with respect to the calcite, as a result of its effective adsorption on such substrate.

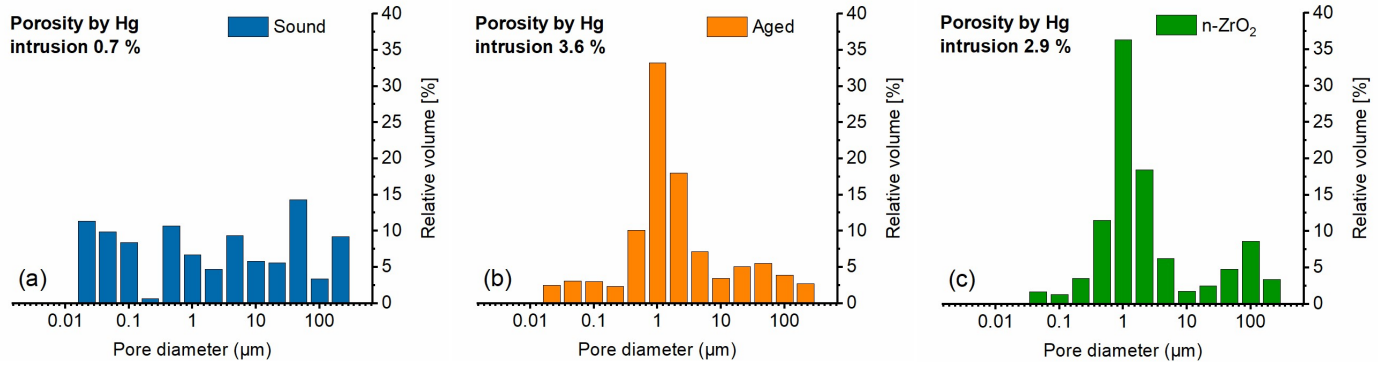

Figure 6. Mercury intrusion porosimetry data displaying the pore radii distribution of Apuan marble in three conditions: (**a**) sound, (**b**) artificially aged or heat treated, and (**c**) artificially aged and consolidated with n-ZrO_2. The open total porosity measured by means of Hg intrusion is also displayed in the graphs for all stone conditions.

3.5.3. Mechanical Tests

Apuan marble is considered a very robust building stone in its freshly quarried state. The reason for this lies in its metamorphic nature, which involves calcite recrystallisation under high pressure, resulting in the formation of strongly interlocking crystals. Therefore, it has almost no water absorption capabilities and a high mechanical strength, as shown by, e.g., the longitudinal dynamic modulus of elasticity obtained from ultrasound probe longitudinal resonance frequency measurements (see Figure 7a, pristine condition 82.7 ± 1.0 GPa ± Std.N.). Only after artificial ageing, porosity in the form of sheet-like openings is generated in the microstructure (see Figure 7a, aged condition 11.6 ± 1.7 GPa ± Std.N.). Restoring the mechanical strength to the marble in such a deteriorated state is very demanding because of the micro-filtering action of the small-sized cracks, inhibiting in-depth penetration of the consolidant and causing its accumulation on the surface and sub-surface regions. The modest increase in dynamic modulus of elasticity upon application of the consolidant onto the aged marble, as determined with a bulk measurement, is clearly shown in Figure 7a (consolidated condition 14.1 ± 0.7 GPa ± Std.N.). The results indicate two important findings: (i) a bulk strengthening of a marble structure cannot be achieved with the applied consolidant and (ii) macroscopic mechanical tests like bending- and splitting-tensile strength are less reliable as the penetration of the entire test specimen with this consolidant cannot be assured.

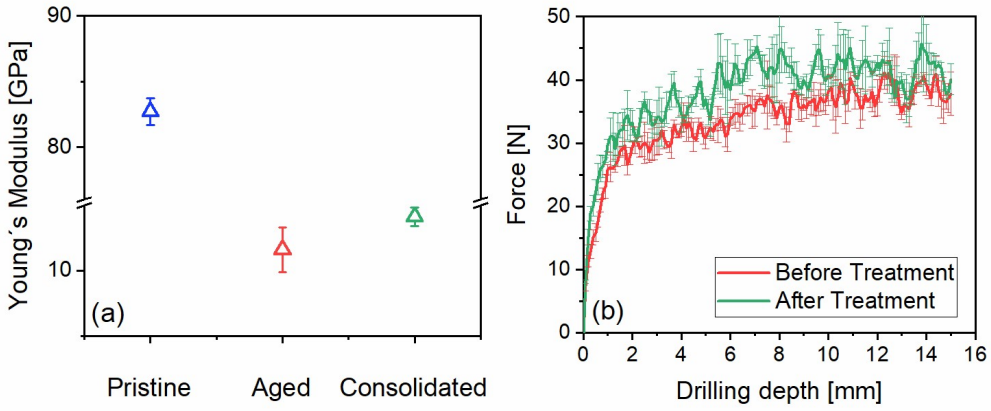

Figure 7. (**a**) Young's modulus in GPa ± Std.N. and (**b**) drilling resistance measurements reported in Newton ± Std.N. before and after treatment.

Since n-ZrO_2 applied on the aged marble should be mainly considered a surface treatment, micro-mechanical tests like the drilling resistance can provide quantitative data about the treatment performance in terms of mechanical gain. Drilling resistance measurements record the force that is required to drill a hole into a material. This can be correlated with the mechanical properties of the material, such as the compressive strength [52]. The drilling resistance of the non-treated artificially aged stone displays a steadily increasing resistance with depth. The reason for such a profile is most probably due to the marble powder resulting from drilling that has been carried along the drilling depth, which increases the resistance progressively. Such a phenomenon has been described previously in other studies concerning the drilling resistance of natural stones [53]. After the treatment with n-ZrO_2, an increase in resistance can be recorded, and it amounts to approx. 13 ± 5% (calculated for the force recorded between 3- and 10-mm depth). The increase in resistance of ~13% on average can be considered appropriate as the n-ZrO_2 is not a structural strengthener but is focused on the surface and sub-surface region. It should be noted that the particle diameter has a significant impact on the performance of particle-based treatments, as was recently demonstrated for nanosilica consolidants [54]. Dziadkowiec et al. demonstrated that smaller nanoparticles yielded stronger adhesive and cohesive interactions when compared with larger ones. In the case of n-ZrO_2, our adsorption studies provide indirect but substantial evidence of the good chemical affinity and effective physical interaction between n-ZrO_2 particles and the calcite substrate. To obtain more details on the impact of particle diameter and particle size distribution, additional research, including the synthesis of such n-ZrO_2 varieties, would be necessary. Moreover, in order to evaluate the effectiveness of the consolidant, additional bulk mechanical tests are required.

3.5.4. Water-Related Tests and Colour Measurements

The colour measurement is described through dE*, the metric difference or distance between two colours according to the rules of the International Commission on Illumination (CIE). In this study, it is used to quantify the colour change between untreated and treated artificially aged samples; acceptable treatments are considered those resulting in dE* < 5 [55]. The axis in the diagram for dE* is set to the highest value obtained, which is 7.56 ± 0.32 for the treatment with n-ZrO_2 (see Figure 8). Among the different measured parameters, the one showing the largest variation is dL*, for which some whitening of the surface could be observed. However, the change in colour might be tackled with appropriate aftercare (e.g., dabbing of excess consolidant from the surface, foil coverage to

prevent quick evaporation and back migration to the surface, cleaning of cured consolidant, etc.), which was not considered in the present research.

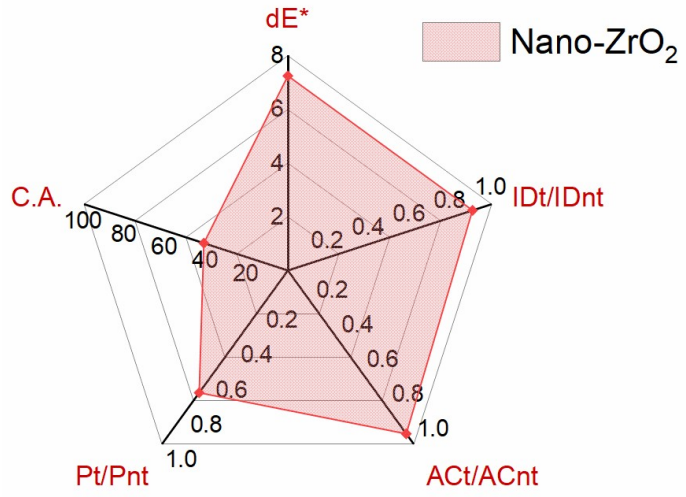

Figure 8. Compatibility assessment of n-ZrO_2 applied on Apuan marble. dE* describes the metric difference or distance between two colours according to the rules of the International Commission on Illumination (CIE). IDt/IDnt represents the ratio of the drying index after a period of 24 h. ACt/ACnt is the ratio of the water absorption coefficient by capillarity after 60 min. Pt/Pnt is the ratio of water vapour permeability. C.A. is the contact angle after treatment. The values for drying index, water absorption coefficient, and water vapour permeability hold the subscript (t) for treated and (nt) for not treated. All corresponding raw data can be viewed in Table 3.

Table 3. Laboratory-based test methods used to assess the compatibility of n-ZrO_2 on Apuan marble in terms of water-related tests and colour measurements. Not treated corresponds to the artificially aged or heat-treated condition, and treated corresponds to the artificially aged and subsequently n-ZrO_2-treated condition.

dE * metric difference between two colours	**L/nt**	**a/nt**	**b/nt**
	79.86 ± 0.14	−1.03 ± 0.07	−3.37 ± 0.17
	L/t	**a/t**	**b/t**
	87.37 ± 0.45	−0.77 ± 0.12	−2.55 ± 0.06
	ΔL *	**Δa ***	**Δb ***
	7.51 ± 0.30	0.26 ± 0.18	0.82 ± 0.11
IDt/IDnt represents the ratio of the drying index after a period of 24 h	**Not treated**	**Treated**	**IDt/IDnt**
	0.0549 0.0390 0.0654	0.0533 0.0448 0.0391	0.9711 1.1493 0.5975
ACt/ACnt is the ratio of the water absorption coefficient by capillarity after 60 min	**Not treated**	**Treated**	**ACt/ACnt**
	0.601 ± 0.024	0.566 ± 0.018	0.94
Pt/Pnt is the ratio of water vapour permeability	**Not treated**	**Treated**	**Pt/Pnt**
	$1.60 \times 10^{-12} \pm 6.08 \times 10^{-14}$	$1.12 \times 10^{-12} \pm 1.26 \times 10^{-13}$	0.70
C.A. is the contact angle after the treatment	**Not treated**	**Treated**	
	68.89 ± 5.52	41.25 ± 2.21	

Although the colour alterations were above the commonly considered acceptable threshold for built heritage, the moisture-related properties of the marble treated with

n-ZrO_2 were satisfactory. For clarification on how to read the radar diagram in Figure 8 for the water-related properties, on the example of Pt/Pnt, which stands for the ratio of water vapour permeability between treated (t) and not treated (nt) conditions: A value of 1 means unchanged permeability before and after the treatment, which is a favourable condition. A ratio below 1 indicates reduced water vapour permeability after the treatment. A value of 0.8 corresponds to a reduction of 20% in water vapour permeability. The latter is the maximum desired threshold (see Table 2 for the success criterion on treatment performance). A value of 0.5 indicates a reduction by 50%, and a value of 0.3 stands for a reduction by 70%, etc. Values greater than 1 have better water vapour properties after the treatment. A value greater than 1 needs further clarification, as it is rather counterintuitive. However, some studies have reported on better water vapour properties after the treatment (e.g., [56]). IDt/IDnt represents the ratio of the drying index after a period of 24 h. With an average value of 0.9, it can be classified as compatible, as no drastic reduction was recorded. However, it should be noted that the obtained ratios are rather widespread, which might be the result of either stone textural features and/or the treatment. On the contrary, the values of ACt/ACnt, which represent the ratio of the water absorption coefficient by capillarity after 60 min, exhibit narrow distributions. With an average value of 0.94, it can be classified as very good in terms of compatibility. The value for Pt/Pnt of 0.7 is reducing the water vapour permeability to an extent below the desired threshold of 20% [57] (p. 540). C.A. is the contact angle after the treatment, which amounts to 41°, a value that is more hydrophilic than before the treatment (see Table 3). The higher hydrophilicity after the treatment might influence the leaching properties of the ENPs, but more studies are necessary to confirm such a conclusion. In both cases, the C.A. before and after the treatment describes a partially wetting surface condition, and this result indicates no negative effects in terms of compatibility or delayed harmfulness.

4. Outlook on Open Research Agenda

The sorption studies can be viewed as a first approach towards a multi-analytical evaluation of the complex interaction between n-ZrO_2 and a porous calcite substrate. Such methodology provides a basis for future adsorption/desorption studies on the interaction between n-ZrO_2 and calcite and, more generally, for investigations concerning any particle-based treatment applied to a porous substrate. Future studies may involve different sizes of the substrate specimens and solid/liquid ratios, as well as NP concentrations, with varying particle sizes and size distributions and mineral substrates. Stone consolidants commonly applied on calcite substrates include alkoxysilane and hydroxyapatite; however, due to their reactivity, these consolidants cannot be used within the herein-designed sorption studies. Instead, other NPs whose application as conservative treatment in the built cultural heritage has been reported, like $CaCO_3$, TiO_2, or SiO_2, could be used in further sorption studies on calcite substrates.

Dimension stone instead of aggregates could be used as a more realistic approach, representative of facade conditions. Additionally, longer desorption experiments (e.g., weeks, months) should be pursued in order to verify the sustainable effect of our observations on low n-ZrO_2 desorption. Finally, annual rainfall intensities and volume related to different climatic zones, the latter including additional environmental features like, e.g., sun exposure, should be considered in future studies.

As concerns the treatment performance, to the best of our knowledge, the use of n-ZrO_2 as a stone consolidant on marble substrate has never been reported to date, which makes a comparison with common stone consolidants, like alkoxysilanes or hydroxyapatite, difficult. Some general advantages of nanoparticle-based consolidants should be good adhesion to the substrate, low shrinkage and thus less cracking, and good bridging

capacity, among others. Our study showed that the consolidant resulted in a poor in-depth penetration in the case of Apuan marble used as a substrate. On the contrary, we observed good moisture-related properties and a good affinity between the n-ZrO_2 and calcite substrate. Alkoxysilanes are known to have a poor adhesion to carbonate substrates, small bridging capacities, and high shrinkage accompanied by cracking [58]. Main advantages of alkoxysilanes include a homogeneous in-depth distribution and good strengthening capacity. The most important advantage of hydroxyapatite is the possibility to tailor its strengthening capacity [59], allowing its use as a consolidant and protective coating [60]. Disadvantages of alkoxysilanes and hydroxyapatite are their curing time. For a comparison between n-ZrO_2 and commonly used stone consolidants, more studies including bulk mechanical tests and different substrates are necessary.

All in all, the proposed multi-characterisation approach (spanning from micro- to macro-) would help to establish guidelines and protocols for future studies regarding both the performance of the treatment and the possible undesired effects, such as, e.g., the leaching of NPs used as consolidants and protectives from building surfaces.

5. Conclusions

This is the first experimental study that verifies the efficiency of a water-based n-ZrO_2 dispersion for strengthening and protecting calcite surfaces. We established the dependence of calcite bead sizes as the key parameter determining the effectiveness of the sorption of the consolidant. n-ZrO_2 effectively adsorbs and remains on the calcite surface, even when exposed to simulated rainwater. This affinity significantly reduces the calcite dissolution, highlighting the potential of n-ZrO_2 as a protective agent. Furthermore, good compatibility is indicated due to slight changes in water-related tests after treatment application. In addition, a slight improvement of the mechanical strength was observed, although only modest n-ZrO_2 penetration could be achieved, depending on the pore size structure of the marble. The study provides a guideline for future studies in the field of built heritage, proving the advantages of combining sorption experiments with mechanical, physical, and optical characterisations.

Supplementary Materials: The following supporting information can be downloaded at: https://www.mdpi.com/article/10.3390/buildings15030492/s1, Figure S1: SEM-EDX analysis of the crystalized efflorescence on top of the cured Nano-Zirconia as applied on Apuan Marble (EDS Spot 1) and SEM-EDX analysis of the cured Nano-Zirconia as applied on Apuan Marble (EDS Spot 2).

Author Contributions: Conceptualization, M.U. and T.G.-D.; methodology, M.U. and T.G.-D.; formal analysis, M.U. and T.G.-D.; investigation, M.U. and T.G.-D.; resources, J.L. and V.C.; data curation, M.U. and T.G.-D.; writing—original draft preparation, M.U. and T.G.-D.; writing—review and editing, J.L. and V.C.; visualization, M.U.; supervision, J.L. and V.C. All authors have read and agreed to the published version of the manuscript.

Funding: This research received no external funding.

Data Availability Statement: The datasets used and/or analyzed during the current study are available from the corresponding author upon reasonable request. The data are not publicly available as they form part of an ongoing study. Additional electronic supplementary material is accompanied by this paper.

Acknowledgments: We gratefully acknowledge the Institute for Nuclear Waste Disposal from the Karlsruhe Institute of Technology for hosting this research project and the unrestricted access to various analysis. The authors further thank the Opera della Primaziale Pisana team from Pisa, Italy, for the supply of the freshly quarried Apuan marble and Technologia Navarra de Nanoproductos, S.L.-Tecnan (Spain) for the supplied consolidant ZR110 (also known under the abbreviation NC-29C). Alberto Viani from the Institute of Theoretical and Applied Mechanics of the Czech Academy of

Sciences is gratefully acknowledged for hosting the SEM analyses. We thank Thomas Kasel (MPA) for the BET analysis and Frank Geyer (KIT-INE) for the help with ICP-MS.

Conflicts of Interest: The authors declare no conflicts of interest.

References

1. Verges-Belmin, V. *Illustrated Glossary on Stone Deterioration Patterns*; ICOMOS-ISCS (International Scientific Committee for Stone): Paris, France, 2008.
2. Sena da Fonseca, B. Current Trends in Stone Consolidation Research: An Overview and Discussion. *Buildings* **2023**, *13*, 403. [CrossRef]
3. Wheeler, G.; Goins, E.S. *Alkoxysilanes and the Consolidation of Stone*; Getty Publications: Los Angeles, CA, USA, 2005.
4. Burgos-Ruiz, M.; Elert, K.; Ruiz-Agudo, E.; Colfen, H.; Rodriguez-Navarro, C. Silica-Functionalized Nanolimes for the Conservation of Stone Heritage. *Small* **2023**, *19*, e2300596. [CrossRef]
5. Gkrava, E.; Tsiridis, V.; Manoudis, P.; Zorba, T.; Pavlidou, E.; Konstantinidis, A.; Karapantsios, T.D.; Spathis, P.K.; Karapanagiotis, I. A robust superhydrophobic coating of siloxane resin and hydrophobic calcium carbonate nanoparticles for limestone protection. *Mater. Today Commun.* **2024**, *38*, 108393. [CrossRef]
6. He, J.; Otero, J.; Crespo-López, L.; Monasterio-Guillot, L.; Benavides-Reyes, C.; Elert, K.; Rodriguez-Navarro, C. Ethyl silicate–nanolime treatment for the consolidation of calcareous building materials. *Constr. Build. Mater.* **2024**, *418*, 135437. [CrossRef]
7. Li, L.; Yang, Q. *Advanced Coating Materials*; John Wiley & Sons: Hoboken, NJ, USA, 2018.
8. Gherardi, F.; Maravelaki, P.N. Advances in the application of nanomaterials for natural stone conservation. *RILEM Tech. Lett.* **2022**, *7*, 20–29. [CrossRef]
9. Mandal, S.; Kumar, P.; Satpathy, B.; Das, K.; Das, S. Nanostructured metal oxide based coating for the protection and conservation of cultural heritage: A comprehensive review. *J. Cult. Herit.* **2024**, *69*, 94–112. [CrossRef]
10. Ban, M.; Aliotta, L.; Gigante, V.; Mascha, E.; Sola, A.; Lazzeri, A. Distribution depth of stone consolidants applied on-site: Analytical modelling with field and lab cross-validation. *Constr. Build. Mater.* **2020**, *259*, 120394. [CrossRef]
11. Chelazzi, D.; Baglioni, P. From Nanoparticles to Gels: A Breakthrough in Art Conservation Science. *Langmuir* **2023**, *39*, 10744–10755. [CrossRef] [PubMed]
12. Ševčík, R.; Viani, A.; Machová, D.; Lanzafame, G.; Mancini, L.; Appavou, M.-S. Synthetic calcium carbonate improves the effectiveness of treatments with nanolime to contrast decay in highly porous limestone. *Sci. Rep.* **2019**, *9*, 15278. [CrossRef] [PubMed]
13. Sierra-Fernandez, A.; Gomez-Villalba, L.S.; Rabanal, M.E.; Fort, R. New nanomaterials for applications in conservation and restoration of stony materials: A review. *Mater. Constr.* **2017**, *67*, e107. [CrossRef]
14. Rashad, A.M.; Eessaa, A.K.; Khalil, M.H.; Mohamed, O.A. An initial study on the effect of nano-zirconium on the behavious of alkali-activated slag cement subjected to seawater attack. *Constr. Build. Mater.* **2023**, *370*, 130659. [CrossRef]
15. Chitoria, A.K.; Mir, A.; Shah, M.A. A review of ZrO_2 nanoparticles applications and recent advancements. *Ceram. Int.* **2023**, *49*, 32343–32358. [CrossRef]
16. Kannan, G.; O'Kelly, B.C.; Sujatha, E.R. Geotechnical investigation of low-plasticity organic soil treated with nano-calcium carbonate. *J. Rock. Mech. Geotech. Eng.* **2023**, *15*, 500–509. [CrossRef]
17. Scherer, G.W.; Wheeler, G.S. Silicate Consolidants for Stone. *Key Engineering Materials* **2009**, *391*, 1–25. [CrossRef]
18. Huang, X.; Auffan, M.; Eckelman, M.J.; Elimelech, M.; Kim, J.-H.; Rose, J.; Zuo, K.; Li, Q.; Alvarez, P.J.J. Trends, risks and opportunities in environmental nanotechnology. *Nat. Rev. Earth Environ.* **2024**, *5*, 572–587. [CrossRef]
19. Selçuk, S.A.; Ayçam, İ. Nanotechnology in Built Environment: Pros and Cons of Nanomaterial Usage in Architecture. In *Proceedings of the 3rd International Sustainable Buildings Symposium, Proceedings of 3rd International Sustainable Buildings Symposium (ISBS), Dubai, UAE, 15–17 March 2017*; Springer: Berlin/Heidelberg, Germany, 2017; pp. 269–281.
20. Brunelli, A.; Calgaro, L.; Semenzin, E.; Cazzagon, V.; Giubilato, E.; Marcomini, A.; Badetti, E. Leaching of nanoparticles from nano-enabled products for the protection of cultural heritage surfaces: A review. *Environ. Sci. Eur.* **2021**, *33*, 48. [CrossRef]
21. Reyes-Estebanez, M.; Ortega-Morales, B.O.; Chan-Bacab, M.; Granados-Echegoyen, C.; Camacho-Chab, J.C.; Pereañez-Sacarias, J.E.; Gaylarde, C. Antimicrobial engineered nanoparticles in the built cultural heritage context and their ecotoxicological impact on animals and plants: A brief review. *Herit. Sci.* **2018**, *6*, 52. [CrossRef]
22. Shandilya, N.; Le Bihan, O.; Bressot, C.; Morgeneyer, M. Emission of titanium dioxide nanoparticles from building materials to the environment by wear and weather. *Environ. Sci. Technol.* **2015**, *49*, 2163–2170. [CrossRef] [PubMed]
23. Fiorentino, B.; Golanski, L.; Guiot, A.; Damlencourt, J.-F.; Boutry, D. Influence of paints formulations on nanoparticles release during their life cycle. *J. Nanopart. Res.* **2015**, *17*, 149. [CrossRef]
24. Kaegi, R.; Sinnet, B.; Zuleeg, S.; Hagendorfer, H.; Mueller, E.; Vonbank, R.; Boller, M.; Burkhardt, M. Release of silver nanoparticles from outdoor facades. *Environ. Pollut.* **2010**, *158*, 2900–2905. [CrossRef] [PubMed]

25. Blocken, B.; Carmeliet, J. A simplified numerical model for rainwater runoff on building facades: Possibilities and limitations. *Build. Environ.* **2012**, *53*, 59–73. [CrossRef]
26. Domercq, P.; Praetorius, A.; Boxall, A.B. Emission and fate modelling framework for engineered nanoparticles in urban aquatic systems at high spatial and temporal resolution. *Environ. Sci. Nano* **2018**, *5*, 533–543. [CrossRef]
27. Kurwadkar, S.; Pugh, K.; Gupta, A.; Ingole, S. Nanoparticles in the environment: Occurrence, distribution, and risks. *J. Hazard. Toxic. Radioact. Waste* **2015**, *19*, 04014039. [CrossRef]
28. Bottero, J.-Y.; Auffan, M.; Borschnek, D.; Chaurand, P.; Labille, J.; Levard, C.; Masion, A.; Tella, M.; Rose, J.; Wiesner, M.R. Nanotechnology, global development in the frame of environmental risk forecasting. A necessity of interdisciplinary researches. *Comptes Rendus Geosci.* **2015**, *347*, 35–42. [CrossRef]
29. Hennebert, P.; Avellan, A.; Yan, J.; Aguerre-Chariol, O. Experimental evidence of colloids and nanoparticles presence from 25 waste leachates. *Waste Manag.* **2013**, *33*, 1870–1881. [CrossRef]
30. Gomez-Villalba, L.S.; Salcines, C.; Fort, R. Application of Inorganic Nanomaterials in Cultural Heritage Conservation, Risk of Toxicity, and Preventive Measures. *Nanomaterials* **2023**, *13*, 1454. [CrossRef] [PubMed]
31. Geissen, V.; Mol, H.; Klumpp, E.; Umlauf, G.; Nadal, M.; van der Ploeg, M.; van de Zee, S.E.A.T.M.; Ritsema, C.J. Emerging pollutants in the environment: A challenge for water resource management. *Int. Soil. Water Conserv. Res.* **2015**, *3*, 57–65. [CrossRef]
32. Azimzada, A.; Farner, J.M.; Hadioui, M.; Liu-Kang, C.; Jreije, I.; Tufenkji, N.; Wilkinson, K.J. Release of TiO2 nanoparticles from painted surfaces in cold climates: Characterization using a high sensitivity single-particle ICP-MS. *Environ. Sci. Nano* **2020**, *7*, 139–148. [CrossRef]
33. Danelska, A.; Ulkowska, U.; Socha, R.P.; Szafran, M. Surface properties of nanozirconia and their effect on its rheological behaviour and sinterability. *J. Eur. Ceram. Soc.* **2013**, *33*, 1875–1883. [CrossRef]
34. Xie, Z.; Ma, J.; Xu, Q.; Huang, Y.; Cheng, Y.-B. Effects of dispersants and soluble counter-ions on aqueous dispersibility of nano-sized zirconia powder. *Ceram. Int.* **2004**, *30*, 219–224. [CrossRef]
35. Hennebert, P.; Anderson, A.; Merdy, P. Mineral Nanoparticles in Waste: Potential Sources, Occurrence in Some Engineered Nanomaterials Leachates, Municipal Sewage Sludges and Municipal Landfill Sludges. *J. Biotechnol. Biomater.* **2017**, *7*, 1000261. [CrossRef]
36. Karunakaran, G.; Suriyaprabha, R.; Manivasakan, P.; Yuvakkumar, R.; Rajendran, V.; Kannan, N. Impact of nano and bulk ZrO2, TiO2 particles on soil nutrient contents and PGPR. *J. Nanosci. Nanotechnol.* **2013**, *13*, 678–685. [CrossRef] [PubMed]
37. Jangra, S.L.; Stalin, K.; Dilbaghi, N.; Kumar, S.; Tawale, J.; Singh, S.P.; Pasricha, R. Antimicrobial activity of zirconia (ZrO_2) nanoparticles and zirconium complexes. *J. Nanosci. Nanotechnol.* **2012**, *12*, 7105–7112. [CrossRef]
38. Herz, N.; Dean, N.E. Stable isotopes and archaeological geology: The Carrara marble, northern Italy. *Appl. Geochem.* **1986**, *1*, 139–151. [CrossRef]
39. Cantisani, E.; Pecchioni, E.; Fratini, F.; Garzonio, C.A.; Malesani, P.; Molli, G. Thermal stress in the Apuan marbles: Relationship between microstructure and petrophysical characteristics. *Int. J. Rock. Mech. Min.* **2009**, *46*, 128–137. [CrossRef]
40. Franzoni, E.; Sassoni, E.; Scherer, G.W.; Naidu, S. Artificial weathering of stone by heating. *J. Cult. Herit.* **2013**, *14*, E85–E93. [CrossRef]
41. Ban, M.; Baragona, A.; Ghaffari, E.; Weber, J.; Rohatsch, A. Artificial Aging Techniques on Various Lithotypes for Testing of Stone Consolidants. In *Proceedings of Science and Art: A Future for Stone, Proceedings of the 13th International Congress on the Deterioration and Conservation of Stone, Paisley, UK, 6–10 September 2016*; Hughes, J., Howind, T., Eds.; University of the West of Scotland: Paisley, UK, 2016; Volume 1, pp. 253–260.
42. Carroll, D. *Rainwater as a Chemical Agent of Geologic Processes: A Review*; US Government Printing Office: Washington, DC, USA, 1962.
43. *EN 14146*; Determination of Dynamic Elastic Modulus by Measuring the Fundamental Resonant Frequency. CEN: Brussels, Belgium, 2004.
44. *EN 15803*; Conservation of Cultural Property-Test Methods-Determination of Water Vapour Permeability. CEN: Brussels, Belgium, 2010.
45. *EN 15801*; Conservation of Cultural Property. Determination of Water Absorption by Capillarity. CEN: Brussels, Belgium, 2010.
46. *EN 16322*; Conservation of Cultural Heritage. Determination of Drying Properties. CEN: Brussels, Belgium, 2013.
47. *EN 15802*; Conservation of Cultural Property. Determination of Static Contact Angle. Ente Nazionale Italiano di Unificazione: Milano, Italy, 2010.
48. *EN 15886*; Conservation of Cultural Property. Colour Measurement of Surfaces. CEN: Brussels, Belgium, 2010.
49. Calia, A.; Lettieri, M.; Masieri, M.; Pal, S.; Licciulli, A.; Arima, V. Limestones coated with photocatalytic TiO 2 to enhance building surface with self-cleaning and depolluting abilities. *J. Clean. Prod.* **2017**, *165*, 1036–1047. [CrossRef]
50. Sena da Fonseca, B.; Ferreira Pinto, A.P.; Rodrigues, A.; Piçarra, S.; Santos, C.; Montemor, M.F. Effect of the pore network and mineralogy of stones on the behavior of alkoxysilane-based consolidants. *Constr. Build. Mater.* **2022**, *345*, 128383. [CrossRef]

51. Ban, M.; Luxbacher, T.; Lützenkirchen, J.; Viani, A.; Bianchi, S.; Hradil, K.; Rohatsch, A.; Castelvetro, V. Evolution of calcite surfaces upon thermal decomposition, characterized by electrokinetics, in-situ XRD, and SEM. *Colloids Surf. A Physicochem. Eng. Asp.* **2021**, *624*, 126761. [CrossRef]
52. Pamplona, M.; Kocher, M.; Snethlage, R.; Barros, L.A. Drilling resistance: Overview and outlook. *Z. Dtsch. Ges. Geowiss.* **2007**, *158*, 665–679. [CrossRef]
53. Sena da Fonseca, B.; Pinto, A.P.F.; Rodrigues, A.; Piçarra, S.; Fonseca, D.; Montemor, M.F. On the estimation of marbles weathering by thermal action using drilling resistance. *J. Build. Eng.* **2021**, *42*, 102494. [CrossRef]
54. Dziadkowiec, J.; Cheng, H.W.; Ludwig, M.; Ban, M.; Tausendpfund, T.P.; von Klitzing, R.; Mezger, M.; Valtiner, M. Cohesion Gain Induced by Nanosilica Consolidants for Monumental Stone Restoration. *Langmuir* **2022**, *38*, 6949–6958. [CrossRef] [PubMed]
55. Sassoni, E.; Graziani, G.; Franzoni, E. An innovative phosphate-based consolidant for limestone. Part 1: Effectiveness and compatibility in comparison With ethyl silicate. *Constr. Build. Mater.* **2016**, *102*, 918–930. [CrossRef]
56. Gherardi, F.; Roveri, M.; Goidanich, S.; Toniolo, L. Photocatalytic Nanocomposites for the Protection of European Architectural Heritage. *Materials* **2018**, *11*, 65. [CrossRef]
57. Snethlage, R.; Sterflinger, K. Stone Conservation. In *Stone in Architecture: Properties, Durability*, 4th ed.; Siegesmund, S., Snethlage, R., Eds.; Springer: Berlin/Heidelberg, Germany, 2011; pp. 411–544. [CrossRef]
58. Rodrigues, A.; Sena da Fonseca, B.; Ferreira Pinto, A.P.; Piçarra, S.; Montemor, M.F. Tailoring alkoxysilanes with poly(ethylene glycol) as potential consolidants for carbonate stones. *Constr. Build. Mater.* **2021**, *289*, 123048. [CrossRef]
59. Sena da Fonseca, B.; Ferreira Pinto, A.P.; Rodrigues, A.; Rucha, M.; Montemor, M.F. Ability of novel consolidants to improve cohesion of carbonate stones: Dependence on pore-shape, aging conditions and treatment procedures. *J. Cult. Herit.* **2022**, *55*, 95–106. [CrossRef]
60. Sassoni, E. Hydroxyapatite and Other Calcium Phosphates for the Conservation of Cultural Heritage: A Review. *Materials* **2018**, *11*, 557. [CrossRef] [PubMed]